Bifunctional Gold Nanoshells with a Superparamagnetic Iron Oxide−Silica Core Suitable for Both MR Imaging and Photothermal Therapy

Xiaojun Ji,[†] Ruping Shao,[†] Andrew M. Elliott,[‡] R. Jason Stafford,[‡] Emilio Esparza-Coss,[‡] James A. Bankson,[‡] Gan Liang,[§] Zhi-Ping Luo,[||] Keeseong Park,[⊥] John T. Markert,[⊥] and Chun Li*[,†]

Departments of Experimental Diagnostic Imaging and Imaging Physics, The University of Texas M. D. Anderson Cancer Center, Houston, Texas 77030, Department of Physics, Sam Houston State University, Huntsville, Texas 77341, Microscopy and Imaging Center, Texas A&M University, College Station, Texas 77843, and Department of Physics, The University of Texas at Austin, Austin, Texas 78712

Received: January 10, 2007; In Final Form: February 21, 2007

We describe the synthesis, characterization, and use of hybrid nanoparticles with a superparamagnetic iron oxide (SPIO)−silica core and a gold nanoshell. These multifunctional nanoparticles, designated SPIO−Au nanoshells, displayed superparamagnetic characteristics and a significant absorbance in the near-infrared (NIR) region of the electromagnetic spectrum. In addition, they exhibited high transverse relaxivities, R_2, and a large R_2/R_1 ratio, and therefore, they could be imaged by MRI to obtain T_2-weighted images. Moreover, the SPIO−Au nanoshells showed efficient photothermal effects when exposed to NIR light. The use of SPIO−Au nanoshells, with their combination of unique magnetic and optical properties, should enhance the efficacy of nanoshell-mediated photothermal therapy by making it possible to direct more nanoparticles to tumors through the application of external magnetic field and by permitting real-time in vivo MRI imaging of the distribution of the nanoparticles before, during, and after photothermal therapy.

Introduction

The increasing availability of nanostructures with highly controlled optical properties in the nanometer size range has created widespread interest in the use of nanoparticles in biological systems for diagnostic and therapeutic applications.[1]

Nanoparticles derived from gold provide an attractive system for diagnostic and therapeutic applications owing to their ease of preparation, ready bioconjugation, good biocompatibility, and unique optical properties.[2−6] In particular, gold nanoshells exhibit strong absorbance with tunable wavelength in the near-infrared (NIR) region of the electromagnetic spectrum. Not only can these particles be used in biomedical imaging applications, but more importantly, they are potential candidates for localized photothermal therapy because they mediate strong plasmon-induced surface heat flux upon absorption of NIR light.[6−8]

Another class of inorganic nanoparticles, superparamagnetic iron oxide (SPIO) nanoparticles, has shown great promise in magnetic resonance imaging (MRI).[9,10] SPIO nanoparticles have a high transverse (or spin−spin) relaxivity, R_2, which results in negative contrast on T_2-weighted images. SPIO-enhanced MRI has become an established technique for the imaging of macrophage activity, in particular for the staging of liver tumors and detection of lymph node metastasis; several products for SPIO-enhanced MRI have been approved or are being studied in clinical trials.[9,11,12] Use of SPIO nanoparticles for the imaging of atherosclerotic lesions[13,14] and for monitoring of the in vivo distribution of cellular trafficking[15] is currently being investigated. In addition, magnetic nanoparticles are being studied to determine whether their use as carriers enhances the delivery of therapeutic agents in the presence of an external magnetic field.[16−18] In these systems, therapeutics (e.g., drugs or genes) are attached to the magnetic nanoparticles and injected near the target site. A magnetic field is then applied to the site externally to concentrate the particles at the target site.

In this article, we describe the synthesis, characterization, and use of nanoparticles with an SPIO core and a gold nanoshell. The resulting multifunctional nanomaterial, designated SPIO−Au nanoshells, combines the attractive photothermal properties of gold nanoshells with the magnetic properties of SPIO and thus might be useful for targeted photothermal therapy mediated through an external magnetic field and MRI guidance.

Experimental Section

Materials. Tetraethylorthosilicate (TEOS), 3-aminopropyltrimethoxysilane (APTMS), ammonia solution (30 wt %, 7 mL), tetrakis(hydroxymethyl)phosphonium chloride (THPC), chloroauric acid ($HAuCl_4$), potassium carbonate (K_2CO_3), and formaldehyde (37%) were purchased from Sigma-Aldrich (St. Louis, MO). Water-based super paramagnetic iron oxide (SPIO, γ-Fe_2O_3) particles (EMG 304) were purchased from Ferrotech (Nashua, NH). Purified water (18 MΩ) was obtained from a Milli-Q Synthesis system (Millipore, Billerica, MA).

Synthesis of SPIO−Au Nanoshells. In a typical procedure, 0.2 mL of water-based SPIO (EMG 304) was diluted with 6 mL of 18 MΩ water and 80 mL of absolute ethanol. An aqueous

* Corresponding author address: Department of Experimental Diagnostic Imaging-Box 57, The University of Texas M. D. Anderson Cancer Center, 1515 Holcombe Boulevard, Houston, Texas 77030. Phone: (713) 792-5182. Fax: (713) 794-5456. E-mail: cli@di.mdacc.tmc.edu.

[†] Department of Experimental Diagnostic Imaging, The University of Texas M. D. Anderson Cancer Center.

[‡] Department of Imaging Physics, The University of Texas M. D. Anderson Cancer Center.

[§] Sam Houston State University.

[||] Texas A&M University.

[⊥] The University of Texas at Austin.

10.1021/jp0702245 CCC: $37.00
Published on Web 04/06/2007

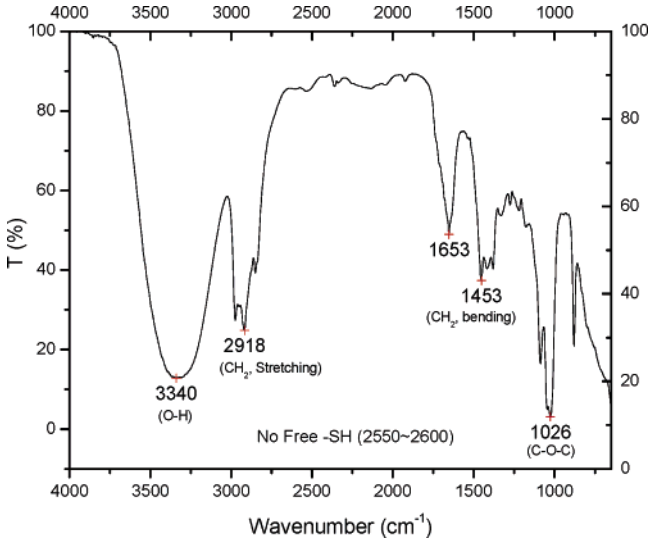

Figure 1. FTIR spectrum of PEG-coated SPIO−Au nanoshells.

ammonia solution (30 wt %, 7 mL) and TEOS (0.5 mL) were consecutively added into the SPIO solution at room temperature under continuous mechanical stirring. The clear solution became a murky suspension in less than 30 min, indicating the formation of silica nanoparticles. The reaction was allowed to proceed at room temperature overnight. The functional groups at the surface of these unmodified silica nanoparticles are predominantly silanol (Si−OH) or ethoxy (Si−OEt) groups.[19] These silica nanoparticles were then treated with 0.04 mL of 3-aminopropyltrimethoxysilane for 6 h to introduce the amino-terminated silica surface, and then the reaction mixture was refluxed for 30 min to complete the reaction.[19] After the reaction mixture had cooled, the SPIO-embedded silica was separated from the reaction medium by centrifugation at 4000 rpm and redispersed in 100 mL of absolute ethanol. Addition of 1 mL of SPIO-embedded silica solution to 5 mL of undiluted THPC gold solution led to the attachment of THPC gold nanocrystals onto the silica surface. This mixture was stored at 4 °C overnight to maximize the surface coverage of the THPC gold nanoseeds. The preparation of THPC gold solution involved the reduction of chloroauric acid ($HAuCl_4$) with THPC, which affords relatively small gold particles (e.g., 2 nm) with a net negative interfacial charge.[20] Finally, the gold nanoshells were prepared by reduction of K-gold solution with formaldehyde (37%) in the presence of SPIO-embedded silica nanoparticles covered with gold nanoseeds. To prepare K-gold solution, 2 mL of 1 wt % $HAuCl_4$ was added to 100 mL of water containing 0.025 g of K_2CO_3 under magnetic stirring. UV−vis absorption spectra were measured 30 min after reaction to verify the formation of nanoshells, which exhibit significant absorbance in the near-infrared region.

Characterization Methods. *Transmission Electron Microscopy (TEM).* To prepare each TEM sample, a small drop of solution was transferred to the top surface of a carbon-film-supported Cu grid (previously glow-discharged to achieve better dispersion) and left until dried. The TEM work was carried out in a microscope (JEOL 2010, JEOL Ltd., Tokyo, Japan) at a working voltage of 200 kV. All imaging magnifications were calibrated using standards of SiC lattice fringes (for high magnifications) and cross-line grating replica (for low magnifications). The size measurements were based on a sufficient number of samples, typically over 30.

Energy-Dispersive Spectroscopy (EDS). EDS was performed using a spectrometer (INCA, Oxford Instruments, Oxon, U.K.) with an ultrathin-window Si−Li detector (capable of detecting elements with $Z \geq 5$) that was attached to a JEOL 2010 microscope.

UV−Vis Spectroscopy. UV−vis spectra of the nanoshells were recorded on a Beckman Coutler DU-800 UV−vis spectrometer (Beckman Coutler, Fullerton, CA) with a quartz cuvette of 10-mm optical path length.

Magnetization Measurements. Magnetization measurements were carried at 300 K in a magnetic field (H) of up to 50 kOe with a superconducting quantum-interference device magnetometer (model MPMS, Quantum Design, San Diego, CA) that can measure magnetic moments as low as 10^{-7} emu. For the magnetization measurements, both uncoated SPIO particles and SPIO−Au nanoshells were in dry powder form obtained by evaporating the water from the solution. The background magnetic moments from the sample capsules (container) were found to be negligible ($\sim 10^{-5}$ emu).

Fourier Transform Infrared (FTIR) Spectroscopy. PEG coating was investigated using a Perkin-Elmer (Wellesley, MA) Spectrum GX system.

Relaxivity. Samples prepared in water at different concentrations (C = 0.00446−0.223 mM) were poured into 4-mm-diameter nuclear magnetic resonance sample tubes (SP Industries, Inc., Warminster, PA). Axial images were obtained using a 4.7-T, 40-cm MR scanner (Bruker Biospin Corp., Billerica, MA) with a 950-mT/m, 5.7-cm-inner-diameter actively shielded gradient coil system [19000 mT/(m s) slew rate] and a 3.5-cm-inner-diameter volume radiofrequency coil. Longitudinal and transverse relaxation studies were performed on axial images acquired with variable-TR (10 TR values ranging from 25 to 3000 ms and TE = 10.5 ms) and variable-TE (24 TE values ranging from 15 to 360 ms and TR = 1000 ms) multislice−multiecho sequences, respectively; other imaging parameters include a 3.2-cm field of view, a 1.0-mm slice thickness, and a 64 × 64 matrix. Regions of interest were used to calculate the signal intensity (SI) at each sample concentration. Plots of TR vs SI and TE vs SI were fit to exponential curves using a custom software program in IDL (ITT Industries, Inc.; Boulder, CO) to provide T_1 and T_2 relaxation constants at each concentration. Then, relaxivities R_1 and R_2 (mM^{-1} s^{-1}) were obtained from linear fitting of the $1/T_1$ vs C and $1/T_2$ vs C plots.

Temperature Elevation Induced by NIR Laser Irradiation. The laser used was a continuous-wave GCSLX-05-1600 m-1 fiber-coupled diode laser (DHC, China Daheng Group, Inc., Beijing, China) with a center wavelength of 808 ± 10 nm. It was powered by a DH 1715A-5 dual-regulated power supply (DHC, China Daheng Group, Inc.). A BioTex LCM-011 optical fiber (5 m in length) was used to transfer laser power from the laser unit to the target. This fiber had a lens mounting at the output that allowed the laser spot size to be changed by changing the distance from the output to the target. The output power was independently calibrated using a handheld optical power meter (Newport model 840-C) and was found to be 1 W for a spot diameter of 3.5 mm and a 2-A supply current. The end of the optical fiber was attached to a retort stand by a movable clamp and positioned directly above the sample cell.

Results and Discussion

Synthesis and PEG Coating of SPIO−Au Nanoshells. The synthesis of the SPIO−Au nanoshells was a multistep procedure (Scheme 1). First, silica-coated SPIO (Fe_2O_3) nanoparticles were synthesized according to the well-known Stöber process.[21] We used commercially available SPIO (average diameter, 10 nm) nanoparticles stabilized with oleic acid in water. The magnetic

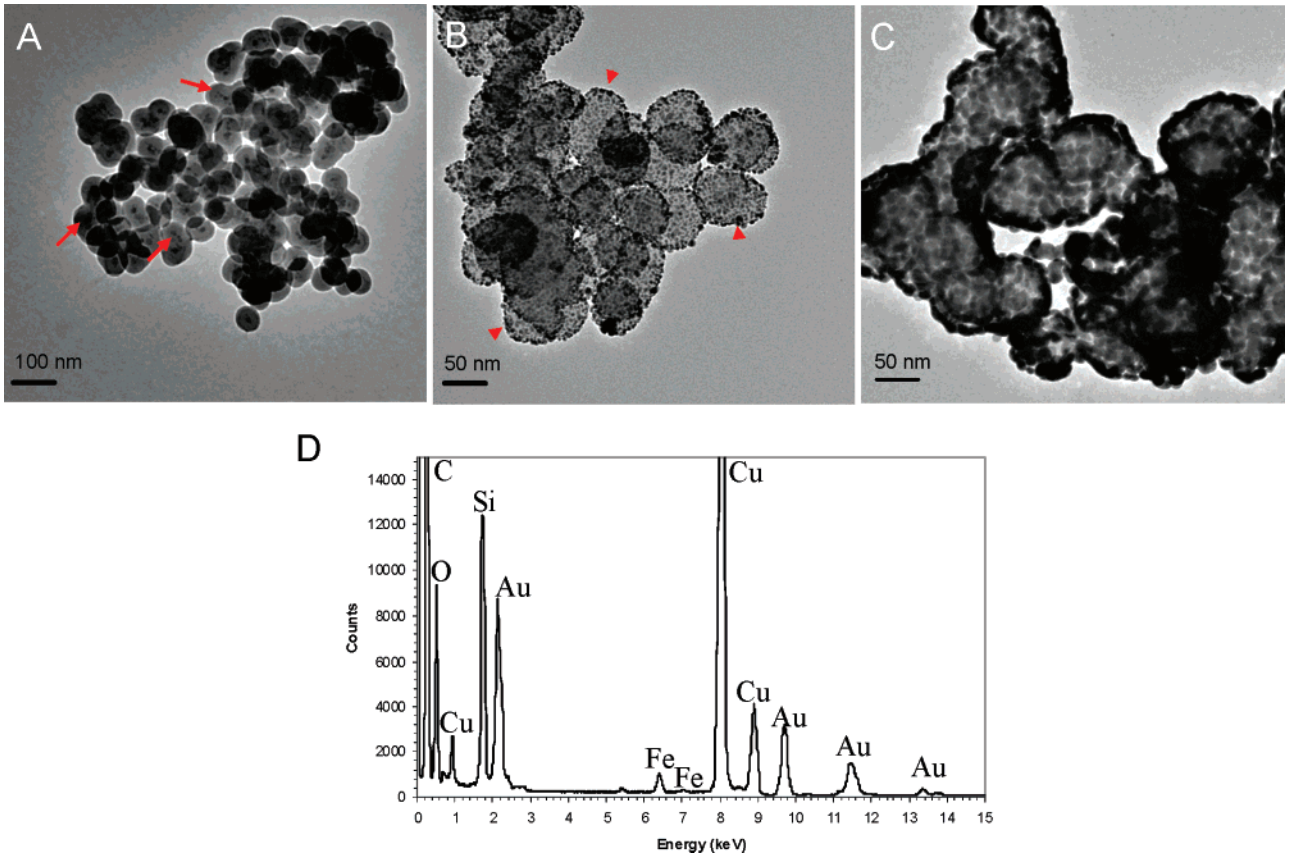

Figure 2. Typical transmission electron microscopy (TEM) images of (A) silica-coated SPIO nanoparticles, (B) silica-coated SPIO nanoparticles with gold nanoseeds on the surface, and (C) SPIO−Au nanoshells. Arrows represent SPIO embedded in silica; arrowheads represent gold nanoseeds. (D) Energy-dispersive spectrum of SPIO−Au nanoshells across the entire image area. The Cu signal is from the Cu grids of the TEM sample.

SCHEME 1: Synthesis of Gold Nanoshells with Superparamagnetic Iron Oxide (SPIO) Cores[a]

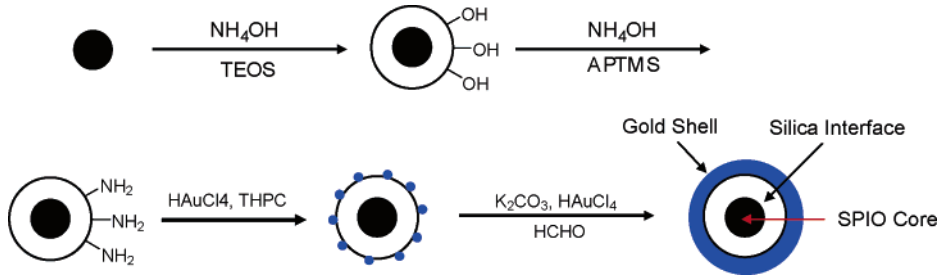

[a] Abbreviations: TEOS, tetraethylorthosilicate; APTMS, 3-aminopropyltrimethoxysilane; THPC, tetrakis(hydroxymethyl)phosphonium chloride.

nanoparticles were easily coated with amorphous silica via the sol−gel process because the iron oxide surface has a strong affinity for silica. No primer was needed to promote the deposition and adhesion of silica. The thickness of the silica sphere could be tuned from 2 to 100 nm simply by changing the concentration of the sol−gel precursor, TEOS.[22] Next, the surface of the silica shell was functionalized with amine groups by treatment with NH_4OH and 3-aminopropyltrimethoxysilane. Then, gold nanocrystal seeds (2−3 nm) were attached to the amino groups on the silica sphere by reduction of chloroauric acid ($HAuCl_4$) with THPC.[23] Because the gold nanoseeds had net negative surface charges, they firmly attached to the amino groups on the silica sphere, which were positively charged at acidic pH. Finally, the attached gold nanoseeds were used to nucleate the growth of a gold overlayer on the silica surface to form a gold nanoshell. The nanoshells were isolated by centrifugation and washed with deionized water. The nanoshells were then resuspended in sodium citrate buffer (33 mM) to stabilize the particle solution. To control the thickness of the gold shells, we varied the concentration of gold-seeded, SPIO-containing silica particles while keeping the concentration of gold precursor ($HAuCl_4$ in 2.5% K_2CO_3 solution) constant.

In our synthesis scheme, the silica layer served the same role as the silica core in conventional gold nanoshells: it provided a dielectric interface for shifting the plasma resonance to the NIR wavelength region. In addition, functionalizing the outer surface of the silica layer with free amine groups facilitated the initial growth of the gold nanoseeds, which, in turn, facilitated the subsequent growth of the outermost gold shell.

In the last step, the nanoshells were coated with polyethylene glycol (PEG) because of its known high biocompatibility. PEG coating was achieved by treating the SPIO−Au nanoshells with monofunctional PEG precursor MeO-PEG-SH (M_w = 5000), resulting in stable nanoparticles. The PEG coating was confirmed using Fourier transform infrared spectroscopy, which showed peaks characteristic of PEG around 2918, 1453, and 1026 cm^{-1} corresponding to the C−H stretching, C−H bending, and C−O stretching vibrations, respectively (Figure 1). We

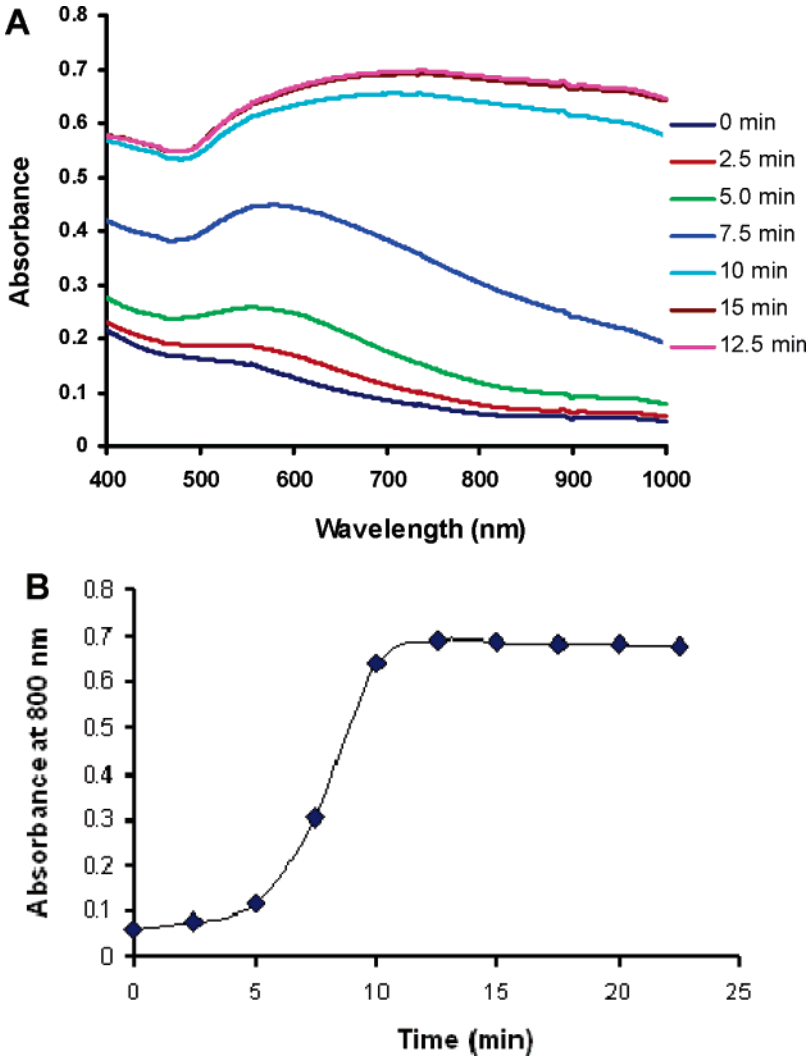

Figure 3. (A) Real-time absorption spectra of SPIO−Au nanoparticles at different times after the addition of K-gold solution and formaldehyde into SPIO−silica nanoparticles with gold nanoseeds. (B) Absorbance of SPIO−Au nanoparticles measured at 800 nm as a function of reaction time after the addition of K-gold solution and formaldehyde.

found that PEG coating afforded nanoshells with good temporal stability. Whereas uncoated nanoshells exhibited a strong tendency toward aggregation (the dispersion became cloudy and began to show signs of settling in minutes), PEG-coated SPIO−Au nanoshells showed no visible signs of aggregation over several weeks of storage at 4 °C.

Characterization of SPIO−Au Nanoshells. Figure 2 shows typical transmission electron microscopy images of nanoparticles at different stages of SPIO−Au nanoshell synthesis. After synthesis of silica-coated SPIO nanoparticles, SPIO nanoparticles (dark contrast) were clearly observed inside the spherical silica (Figure 2A). Most of these particles contained one to four single SPIO nanoparticles or clusters of SPIO nanoparticles. The mean diameter of the silica-coated SPIO nanoparticles was estimated to be 66.0 ± 9.5 nm. After treatment with $HAuCl_4$ and THPC, gold nanoseeds on the silica surface were clearly observed (densely distributed dark spots; Figure 2B). The SPIO−Au nanoshells had an average diameter of 82.2 ± 9.7 nm, and the gold shell had a thickness of ∼8 nm. The gold coating was not continuous, with topographical roughness on the nanometer scale (Figure 2C). Energy-dispersive spectroscopy of the PEG-coated SPIO−Au nanoshells across the entire image area showed the presence of C, O, Si, Fe, and Au (Figure 2D). Absorption spectra of the SPIO−Au nanoshells at different stage of preparation are shown in Figure 3. As the coverage of gold on the SPIO-embedded silica nanoparticles increased, the surface plasmon resonance peak became more prominent and red-shifted toward the NIR region (Figure 3A). The absorbance at 800 nm increased with reaction time and reached a plateaue by 10 min after the addition of K-gold solution (Figure 3B). Theoretical calculations have shown that the plasmon resonance of noble-metal nanoshells can vary over hundreds of nanometers, as the position of the resonance is dictated by both the shell thickness and the size of the dielectric core.[24] The broad absorbance between 700 and 900 nm suggests that the SPIO−Au nanoshells would be suitable for photothermal therapy with light in the NIR region, where there is minimum light absorption in tissues.

Magnetic Properties of SPIO−Au Nanoshells. To determine whether the SPIO−Au nanoshells exhibited magnetic properties that could potentially be used for magnetic-field-guided targeting, we dispersed the SPIO−Au nanoshells in pure water. A Nd−Fe−B magnet (∼0.3 T) was then used to separate the nanoshells. The solution of SPIO−Au nanoshells, which was initially dark, was almost transparent after 15 min of exposure to the magnetic field (Figure 4A,B). The particles were precipitated to one side of the vial wall. UV−vis spectroscopy revealed that more than 85% of the nanoshells were removed from the solution. Figure 4C shows the room-temperature magnetization curve of the SPIO−Au nanoshells obtained using a superconducting quantum-interference device. For comparison,

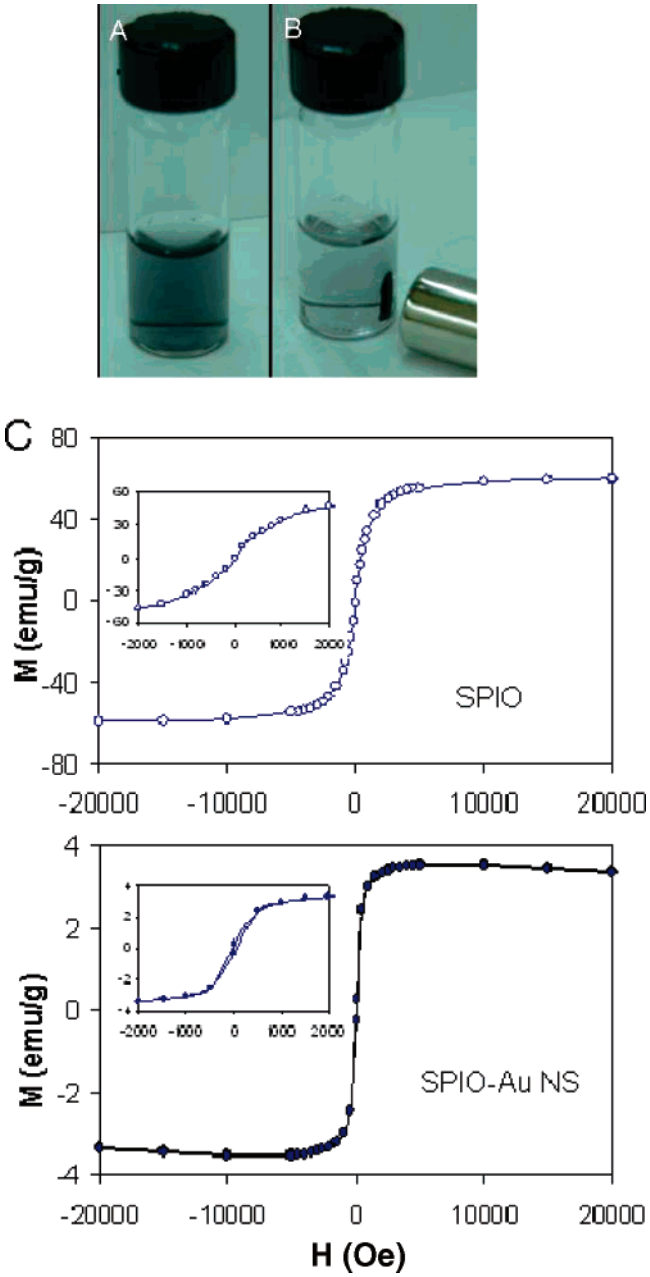

Figure 4. Photographs of a vial containing SPIO−Au nanoshells (1×10^{11} particles/mL) in pure water (A) before and (B) after magnetic separation for 15 min. (C) Magnetization curves of commercial SPIO nanoparticles and SPIO−Au nanoshells measured at 300 K.

TABLE 1: Relaxivities of Various Nanoparticles

nanoparticle	composition	R_2 ($mM^{-1}\ s^{-1}$)	R_1 ($mM^{-1}\ s^{-1}$)	R_2/R_1
SPIO	Fe_2O_3	162	4.4	36.8
SPIO−Au	Fe_2O_3 + silica + Au	369, 11.4	0.02	>10000 at low concentration

the magnetization curve of the commercial SPIO nanoparticles (average diameter, 10 nm) used in the preparation of the SPIO−Au nanoshells is also presented. The insets are plots of $M(H)$ in the enlarged region between −2 and 2 kOe. The $M(H)$ hysteresis loop for the SPIO−Au nanoshells was almost completely reversible, indicating that the SPIO−Au nanoshells exhibit superparamagnetic characteristics (Figure 4C). The saturation moment per unit mass, M_s, for the SPIO−Au nanoshells was 3.5 emu/g at 20 kOe, which is about 5.9% of the M_s for SPIO. The observed M_s value for the SPIO−Au nanoshells agrees well with previously reported data for silica-coated iron oxide nanoparticles (3.6 emu/g).[25] We also measured the magnetic moment of Au−silica nanoshells without SPIO at 1000 Oe, and the results showed that Au−silica nanoshells without SPIO exhibit diamagnetic characteristics with a magnetic moment no more than 0.3% of that of SPIO−Au nanoshells. Taking these results together, we conclude that the decrease in M_s is most likely the result of a large volume of silica/Au in the coated nanoparticles and that the gold and silica layers in SPIO−Au nanoshells do not affect the magnetization saturation of SPIO nanoparticles.

Magnetic Resonance (MR) Relaxation Study of SPIO−Au Nanoshells. Because SPIO nanoparticles are effective T_2 MRI contrast agents,[9,10] we evaluated the T_2 and T_1 relaxations of SPIO−Au nanoshells. Figure 5 shows the results for the relaxivities of SPIO−Au nanoshells for Fe_2O_3 concentrations in the range of 0.00446−0.223 mM measured at 4.7 T at room temperature. Table 1 compares the relaxivities measured for SPIO and SPIO−Au nanoparticles. One of the interesting features observed for the SPIO−Au nanoshells is that their R_2 relaxivity exhibited bilinear behavior, with a 32-fold increase in R_2 at lower concentrations (0.00446−0.0446 mM) compared to that at higher concentrations (0.0446−0.223 mM). In comparison, Kim et al.[26] recently reported linear R_2 relaxivity for a superparamagnetic gold nanoshell sample in which iron oxide nanoparticles were introduced at the interface between the silica and gold layers. The observation of bilinear relaxivity for the SPIO−Au nanoshells might originate from the clusters of SPIO nanoparticles within the silica core of the SPIO−Au nanoshells. A similar bilinear relaxivity behavior has been observed with Gd_3N clusters encapsulated in C_{80} fullerene.[27] Compared to the SPIO precursor used in the preparation of the SPIO−Au nanoshells, the SPIO−Au nanoshells had a significantly increased R_2 relaxivity at lower concentrations but an almost completed suppressed longitudinal relaxavity (R_1) (Figure 5 and Table 1). The amount of Fe_2O_3 in the SPIO−Au nanoshells was estimated from the amount of SPIO initially added into the silica sol−gel solution, assuming a 100% yield of incorporation into the SPIO−Au nanoshells. Therefore, the actual R_2 value might be higher than that reported here because of the possible overestimation of Fe_2O_3 concentrations. Clearly, a detailed study is needed to understand the mechanism responsible for the improved R_2 relaxivity at lower concentrations and reduced R_1 relaxivity in the SPIO−Au nanoshells. Nevertheless, the increased R_2 relaxivity and large R_2/R_1 ratio indicate that the SPIO−Au nanoshells can be used as a contrast agent for obtaining T_2-weighted images at reduced concentrations.

Photothermal Study of SPIO−Au Nanoshells. An important feature of nanoshells is NIR light-induced thermal effect, which could be used for selective treatment of solid tumors.[6−8] To investigate temperature elevation induced by NIR laser irradiation in the presence of SPIO−Au nanoshells, we used a continuous-wave fiber-coupled diode laser with a center wavelength of 808 ± 10 nm. Figure 6A shows the experimental setup. Experiments in aqueous solution showed that the temperature increased with increasing exposure time and plateaued after about 5 min of light exposure (Figure 6B). At a concentration of 7.5×10^{12} particles/mL, an elevation of 16.3 °C was achieved at a power output of 1 W. In comparison, no significant temperature change was observed when pure water or an SPIO−silica dispersion at a concentration of 1.0×10^{13} particles/mL was exposed to the laser light. These data indicate that the SPIO−Au nanoshells acted as an efficient photothermal media-

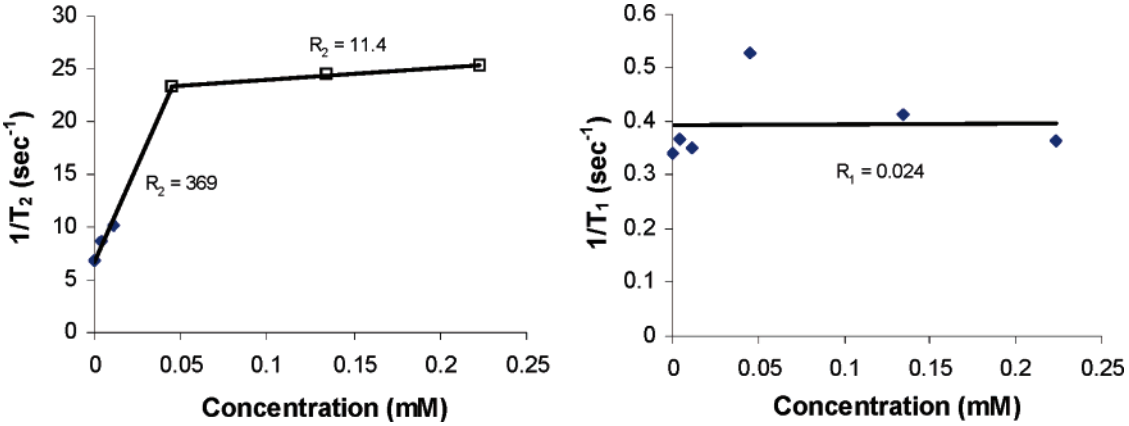

Figure 5. Graph of relaxivities of SPIO−Au nanoshells at concentrations from 0.00446 to 0.223 mM at 4.7 T (room temperature). Bilinear behavior is observed with increased R_2 relaxivity at the lowest concentration levels. Note the absence of longitudinal relaxivity R_1.

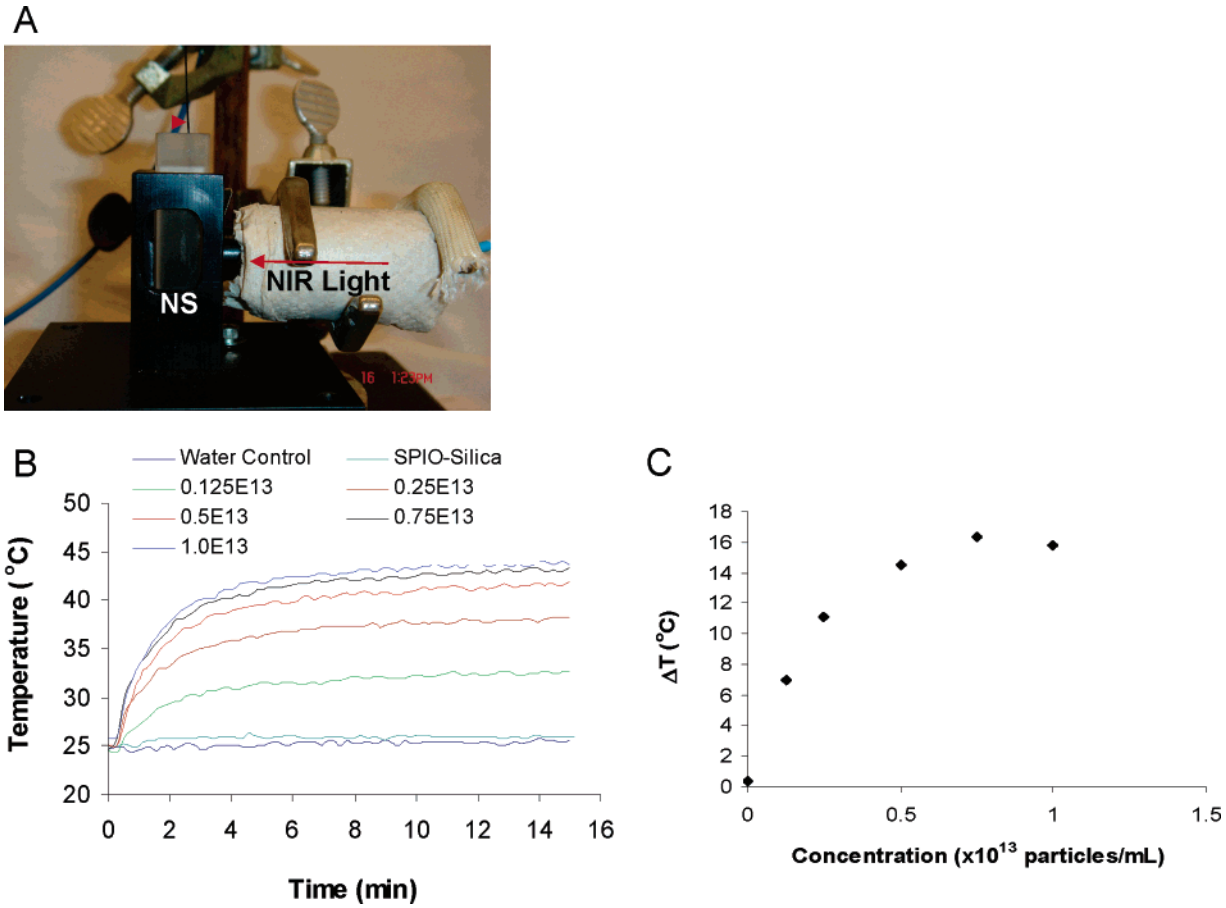

Figure 6. (A) Photograph of the experimental setup for measuring temperature changes mediated by SPIO−Au nanoshells. NS indicates the aqueous solution containing the nanoshells in a quartz cuvette (100 μL), the arrow represents an optical fiber delivering NIR laser light (808 nm) through the cuvette window and the arrowhead indicates the thermocouple. (B) Temperature measured over a period of 15 min of exposure to NIR light at various nanoshell concentrations at an output power of 1 W. Water and SPIO−silica dispersion (1.0×10^{13} particles/mL) were used as controls. (C) Temperature change (ΔT) over a period of 5 min as a function of nanoshell concentration.

tor. It should be noted that the temperature increased with increasing nanoshell concentration at nanoshell concentrations of $<5.0 \times 10^{12}$ particles/mL. At higher concentrations ($>5.0 \times 10^{12}$ particles/mL), no further increase in temperature was observed when the concentration was increased (Figure 6C), suggesting that scattering of light by the nanoshells became a dominant factor at higher concentrations.

Conclusion

In summary, we have succeeded in synthesizing gold nanoshells with an SPIO core. These nanoparticles formed a stable solution in water when coated with PEG; were superparamagnetic; and had high R_2 and R_2/R_1 values, so that they could be imaged by MRI to obtain T_2-weighted images. Moreover, these nanoparticles exhibited strong NIR absorbance and an efficient photothermal effect. These multifunctional SPIO−Au nanoshells should enhance the efficacy of nanoshell-mediated photothermal therapy by making it possible to direct more nanoparticles to tumors through the application of an external magnetic field and by permitting real-time in vivo MRI imaging of the distribution of the nanoparticles before, during, and after photothermal therapy. Further studies to investigate

the in vivo diagnostic and therapeutic potential of this novel material are in progress.

Acknowledgment. The work at U. T. M. D. Anderson Cancer Center was supported by the National Cancer Institute (Grant R01 CA119387) and by the John S. Dunn Foundation. The work at Sam Houston State University was supported by a grant from the SHSU EGR program and by an award from the Research Corporation. The work at University of Texas at Austin was supported by the Welch Foundation under Grant F-1191 and by the National Science Foundation under Grant DMR-0605828. We thank Stephanie Deming for editorial assistance.

References and Notes

(1) Wickline, S. A.; Lanza, G. M. *Circulation* **2003**, *107*, 1092.

(2) Schwartzberg, A.; Olson, T.; Talley, C.; Zhang, J. *J. Phys. Chem. B* **2006**, *110*, 19935.

(3) Schwartzberg, A. M.; Oshiro, T. Y.; Zhang, J. Z.; Huser, T.; Talley, C. E. *Anal. Chem.* **2006**, *78*, 4732.

(4) Sokolov, K.; Follen, M.; Aaron, J.; Pavlova, I.; Malpica, A.; Lotan, R.; Richards-Kortum, R. *Cancer Res.* **2003**, *63*, 1999.

(5) El-Sayed, I. H.; Huang, X.; El-Sayed, M. A. *Nano Lett.* **2005**, *5*, 829.

(6) Loo, C.; Lin, A.; Hirsch, L.; Lee, M. H.; Barton, J.; Halas, N.; West, J.; Drezek, R. *Technol. Cancer Res. Treat.* **2004**, *3*, 33.

(7) Hirsch, L. R.; Stafford, R. J.; Bankson, J. A.; Sershen, S. R.; Rivera, B.; Price, R. E.; Hazle, J. D.; Halas, N. J.; West, J. L. *Proc. Natl. Acad. Sci. U.S.A.* **2003**, *100*, 13549.

(8) O'Neal, D. P.; Hirsch, L. R.; Halas, N. J.; Payne, J. D.; West, J. L. *Cancer Lett.* **2004**, *209*, 171.

(9) Bulte, J. W.; Kraitchman, D. L. *NMR Biomed.* **2004**, *17*, 484.

(10) Wang, Y. X.; Hussain, S. M.; Krestin, G. P. *Eur. Radiol.* **2001**, *11*, 2319.

(11) Tanimoto, A.; Kuribayashi, S. *Eur. J. Radiol.* **2006**, *58*, 200.

(12) Harisinghani, M. G.; Barentsz, J.; Hahn, P. F.; Deserno, W. M.; Tabatabaei, S.; van de Kaa, C. H.; de la Rosette, J.; Weissleder, R. *N. Engl. J. Med.* **2003**, *348*, 2491.

(13) Schmitz, S. A.; Coupland, S. E.; Gust, R.; Winterhalter, S.; Wagner, S.; Kresse, M.; Semmler, W.; Wolf, K. J. *Invest. Radiol.* **2000**, *35*, 460.

(14) Schmitz, S. A.; Taupitz, M.; Wagner, S.; Wolf, K. J.; Beyersdorff, D.; Hamm, B. *J. Magn. Reson. Imaging* **2001**, *14*, 355.

(15) Frank, J. A.; Anderson, S. A.; Kalsih, H.; Jordan, E. K.; Lewis, B. K.; Yocum, G. T.; Arbab, A. S. *Cytotherapy* **2004**, *6*, 621.

(16) Mondalek, F. G.; Zhang, Y. Y.; Kropp, B.; Kopke, R. D.; Ge, X.; Jackson, R. L.; Dormer, K. J. *J. Nanobiotechnol.* **2006**, *4*, 4.

(17) Jain, T. K.; Morales, M. A.; Sahoo, S. K.; Leslie-Pelecky, D. L.; Labhasetwar, V. *Mol. Pharm.* **2005**, *2*, 194.

(18) Morishita, N.; Nakagami, H.; Morishita, R.; Takeda, S.; Mishima, F.; Terazono, B.; Nishijima, S.; Kaneda, Y.; Tanaka, N. *Biochem. Biophys. Res. Commun.* **2005**, *334*, 1121.

(19) Badley, R. D. F. W. T.; McEnroe, F. J.; Assink, R. A. *Langmuir* **1990**, *6*, 792.

(20) Grabar, K. C.; Allison, K. J.; Baker, B. E.; Bright, R. M.; Brown, K. R.; Freeman, R. G.; Fox, A. P.; Keating, C. D.; Musick, M. D.; Natan, M. J. *Langmuir* **1996**, *12*, 2353.

(21) Stöber, W.; Fink, A.; Bohn, E. *J. Colloid Interface Sci*. **1968**, *26*, 62.

(22) Lu, L.; Yin, Y.; Mayers, B.; Xia, Y. *Nano Lett.* **2002**, *2*, 183.

(23) Duff, D. G.; Baiker, A.; Edwards, P. P. *Langmuir* **1993**, *9*, 2301.

(24) Averitt, R.; Sarkar, D.; Halas, N. *Phys. Rev. Lett.* **1997**, *78*, 4217.

(25) Yu, J-H.; Lee, C-W.; Im, S-S.; Lee, J-S. *Rev. Adv. Mater. Sci.* **2003**, *4*, 55.

(26) Kim, J.; Park, S.; Lee, J. E.; Jin, S. M.; Lee, J. H.; Lee, I. S.; Yang, I.; Kim, J. S.; Kim, S. K.; Cho, M. H.; Hyeon, T. *Angew. Chem., Int. Ed.* **2006**, *45*, 7754.

(27) Fatouros, P. P.; Corwin, F. D.; Chen, Z. J.; Broaddus, W. C.; Tatum, J. L.; Kettenmann, B.; Ge, Z.; Gibson, H. W.; Russ, J. L.; Leonard, A. P.; Duchamp, J. C.; Dorn, H. C. *Radiology* **2006**, *240*, 756.